Electronic Supplementary Material (ESI) for Physical Chemistry Chemical Physics.

Supplementary Information

Electric-field control of single-molecule tautomerization

Shai Mangel,[a] Maxim Skripnik,[b,c] Katharina Polyudov,[a] Christian Dette,[a] Tobias Wollandt,[a] Paul Punke,[a] Dongzhe Li,[c] Roberto Urcuyo,[a,†] Fabian Pauly,[b,c] Soon Jung Jung,[a,*] Klaus Kern [a,d]

[a] Max Planck Institute for Solid State Research, Heisenbergstraße 1, 70569 Stuttgart, Germany

[b] Okinawa Institute of Science and Technology Graduate University, Onna-son, Okinawa 904-0495, Japan

[c] Department of Physics, University of Konstanz, 78457 Konstanz, Germany

[d] Institute de Physique, École Polytechnique Fédérale de Lausanne, 1015 Lausanne, Switzerland

*Corresponding Author's e-mail: s.jung@fkf.mpg.de

SI 1: Current-time traces for fixed lateral position

When the measurement method is switched from constant-current mode to constant-height mode, the feedback loop is turned off. At this instant the vertical position of the tip is fixed at either a high or low position above the substrate that depends on the location of the hydrogen atoms in the molecular cavity. Thus, the vertical tip position can produce two different kinds of current-time traces. Figure S1 presents these traces, recorded at the same location above a molecule. The red and white traces correspond to measurements, where the feedback loop was turned off while tunneling occurred into a higher and lower local density of states, respectively. The white (red) current trace in Figure S1 corresponds to a tip position that is closer to (further from) the molecule.

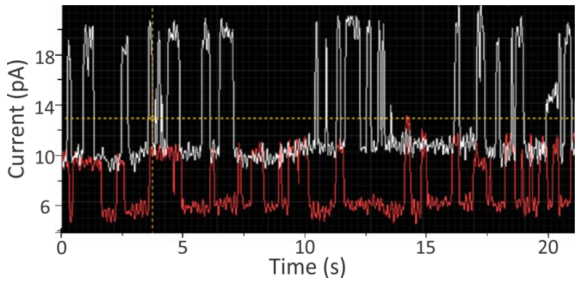

Figure S1: Two kinds of current-time traces, recorded at the same lateral location but at different heights above the molecule.

SI 2: dI/dV spectra of graphene as a function of gate voltage

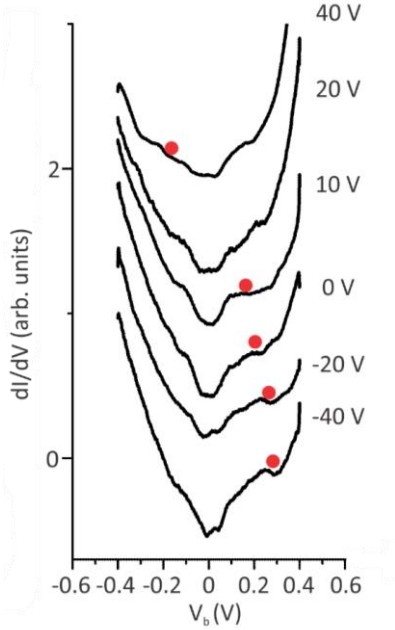

In order to demonstrate the influence of the gate voltage on the charge-carrier concentration in graphene, we took d*I*/d*V* spectra of bare graphene at a fixed spatial location for different gate voltages, as displayed in figure S2. Each spectrum was measured between -400 mV≤V_b≤400 mV and shows the same characteristic features as previously reported.[1] We have marked the location of the Dirac point by a red dot.

Figure S2: Differential conductance spectra as a function of the applied gate voltage. The position of the Dirac point for each of these spectra is indicated by a red dot. At V_g = 20 V, the Dirac point is positioned in the central gap.

SI 3: Raw data of reaction rates as a function of gate voltage

Figure S3 displays the measured reaction rates of the tautomerization reaction as a function of applied gate voltage. The same set of data, normalized to the maximum value for each molecule, is presented in figure 3a. The variations in the measured frequencies are attributed to the local inhomogeneity and corrugation of the graphene surface, onto which the H_2Pc molecules are deposited.

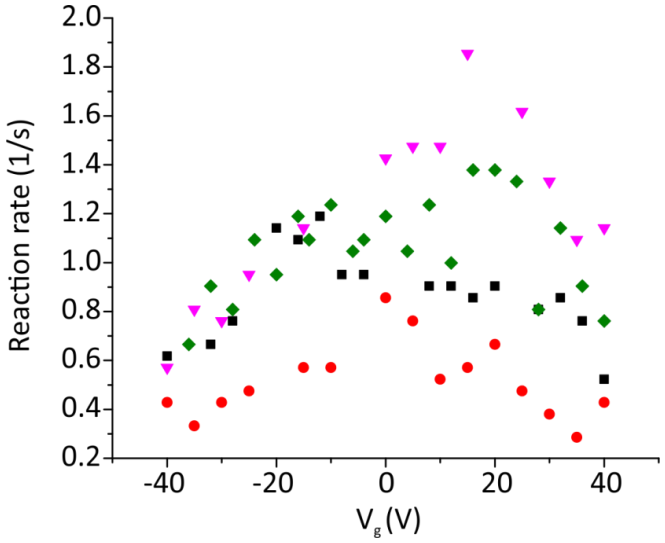

Figure S3: Unnormalized reaction rate as a function of applied gate voltage (V_b=1.6 V, I=10 pA) for four different molecules, as indicated by the different colors.

SI 4: Tip-sample distance as a function of gate voltage

A detailed understanding of the behavior of the tip-sample distance in dependence on the gate voltage can be obtained by studying the well-established Landauer formula. It describes the tunneling current $I(z, V_g, V_b)$ as a function of the tip-sample distance z, the applied bias voltage V_b and the gate voltage V_g:

$$I(z, V_g, V_b) = \frac{2e}{h} \int_{-\infty}^{\infty} T(\varepsilon, z) \rho_{tip}(\varepsilon) \rho_{gr}(\varepsilon - eV_b, V_g) \left(f(\varepsilon, \mu_{gr}(V_b)) - f(\varepsilon, \mu_{tip}) \right) d\varepsilon.$$

Here, $f(\varepsilon, \mu) = \left(1 + \exp((\varepsilon - \mu)/(k_B T))\right)^{-1}$ is the Fermi-Dirac distribution function, ε is the energy of transmitted electrons, μ the electrochemical potential of the respective electrode, $\rho_{gr}(\varepsilon, V_g)$ the density of states (DOS) of graphene,[2] $\rho_{tip}(\varepsilon)$ the DOS of the STM tip, $T(\varepsilon, z)$ the energy- and distance-dependent tunneling probability and $e = |e|$ the elementary charge. Note that V_g and V_b are voltages referenced to the graphene sheet. Since the metallic STM tip is expected to feature a fairly constant DOS in the considered energy range, we assume $\rho_{tip}(\varepsilon) = \rho_{tip} = \text{const}$. Furthermore, the energy dependence of the graphene DOS can be described as $\rho_{gr}(\varepsilon, V_g) = \rho_{gr}\left(\varepsilon - E_D(V_g)\right)$ with the gate-voltage-dependent energy of the Dirac point $E_D(V_g) = \gamma\sqrt{|V_g + V_{sub}|}$. Here, V_{sub} represents a shift caused by substrate doping. From the

experiment we estimate $\gamma \approx 0.033\, e/\sqrt{\mathrm{V}}$ and $V_{\mathrm{sub}} \approx -2$ V. Finally, following the WKB approximation, we assume a tunneling probability of $T(\varepsilon, z) = \exp\left(-2z\sqrt{2m(\Phi - \varepsilon)}/\hbar\right)$, which is valid for a z-independent potential well of $\Phi = 4.9$ eV, and m is the electron mass. By inserting all the relations into the Landauer formula and assuming low temperature, we obtain

$$I(z, V_{\mathrm{g}}, V_{\mathrm{b}}) = \frac{2e}{h}\rho_{\mathrm{tip}} \int_0^{eV_{\mathrm{b}}} \exp\left(-2z\sqrt{2m(\Phi - \varepsilon)}/\hbar\right) \rho_{\mathrm{gr}}\left(\varepsilon - eV_{\mathrm{b}} - \gamma\sqrt{|V_{\mathrm{g}} + V_{\mathrm{sub}}|}\right) d\varepsilon.$$

For a fixed setpoint current I_0, the relation $I(z, V_{\mathrm{g}}, V_{\mathrm{b}}) = I_0$ constitutes an implicit equation $z(I_0, V_{\mathrm{g}}, V_{\mathrm{b}})$, describing the dependence of tip height on the tunneling parameters. Setting $V_b = 1.6\,\mathrm{V}$, as in the experiements and supressing the parameter henceforth, we determine the dependence of tip height on V_g as follows:

1. Compute $I_0 = I(z_0, V_{\mathrm{g}} = 0)$ with the experimental value $z_0 = z(I_0, V_{\mathrm{g}} = 0)$.
2. Search for the root of $I(z, V_{\mathrm{g}}) - I_0 = 0$, e.g. with the bisection method.
3. Repeat step 2 for all V_{g} in the desired range.

The dependence $z(I_0, V_{\mathrm{g}})$ is visualized in figure S4 and agrees qualitatively with the experimental observations in figure 3b.

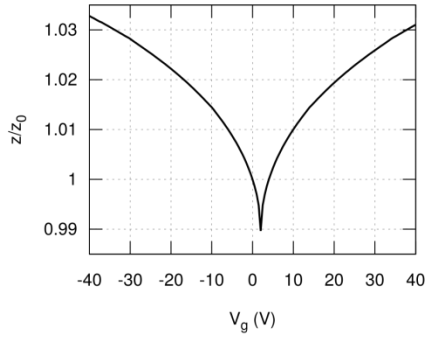

Figure S4: Relative change of the tip-sample distance induced by the applied gate voltage V_{g}.

SI 5: Estimation of the tip-induced electric field

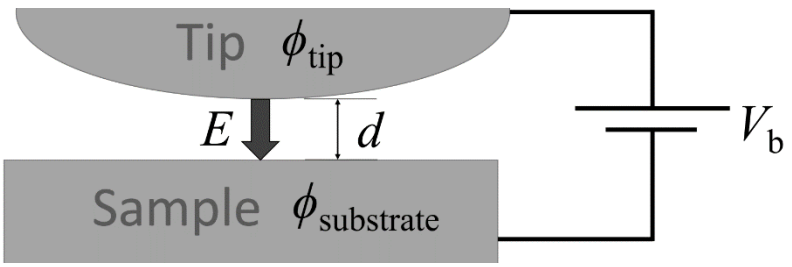

Figure S5: By assuming a simple plate-capacitor model, we estimate the electric field induced by the STM tip to be $E=(V_{\mathrm{b}}+\phi_{\mathrm{tip}}-\phi_{\mathrm{substrate}})/d$.

Employing a bias voltage of V_b=1.6 V, work functions for tip and substrate of $\phi_{tip}=\phi_{PtIr}$=5.2 V and $\phi_{substrate}=\phi_{gr}$=4.6 V, respectively, and the tip-molecule distance d=10 Å, we obtain E=2.2 V/nm.

SI 6: Calculated transition between the tautomers

According to calculations of the minimum-energy path (MEP) the transition between the two *trans* tautomers takes place via one of the two possible cis states. In addition we define a direct path which is obtained via a linear interpolation of the initial and the final trans states. Therefore, the direct path does not involve any sturctural optimizations. Both H atoms move simultaneously along a straight line until they reach the neighboring N atoms, the corresponding potential for such a reaction path is shown in figure S6. It exhibits an energy barrier of 2.8 eV that is much larger than for the corresponding transition via the cis state. A direct transition is therefore improbable due to the relatively high activation energy involved.

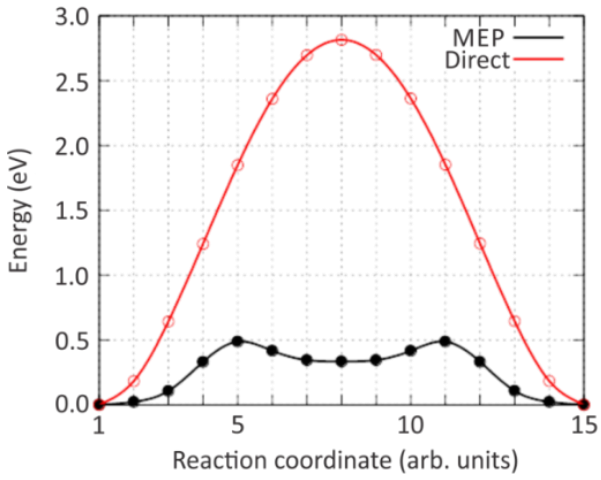

Figure S6: Comparison of the potential energy for the MEP (which proceeds from a trans to a cis to a trans state) and the "direct" path between two trans states (involving the simultaneous motion of the two H atoms between the trans states).

The activation energy that we have calculated is lower than the value of previous work.[3] The difference can be attributed to the difference in the ab-initio approaches as summarised below:

1. The exchange-correlation functional and the basis sets differ.
2. For the MEP calculations, we used the 'nudged-elastic-band method with climbing images', whereas in the reference the barrier has been calculated from the energies of 10 partially optimized structures.
3. The N-H distance was fixed in the reference. However, we do not impose any constraints in the calculations for vanishing E and α.

SI 7: Surface roughness

Although the H_2Pc monolayer on top of the graphene exhibits an average corrugation of 1.9 Å (r.m.s. value in the area of 30 × 30 nm^2), the roughness increases when we consider a smaller area, see figure S7. The maximum tilt angle, which we observe, corresponds to 24.5°. However, this value cannot be directly translated into the tilting angle α of a H_2Pc molecule, because it contains a convolution of topographic and electronic information.

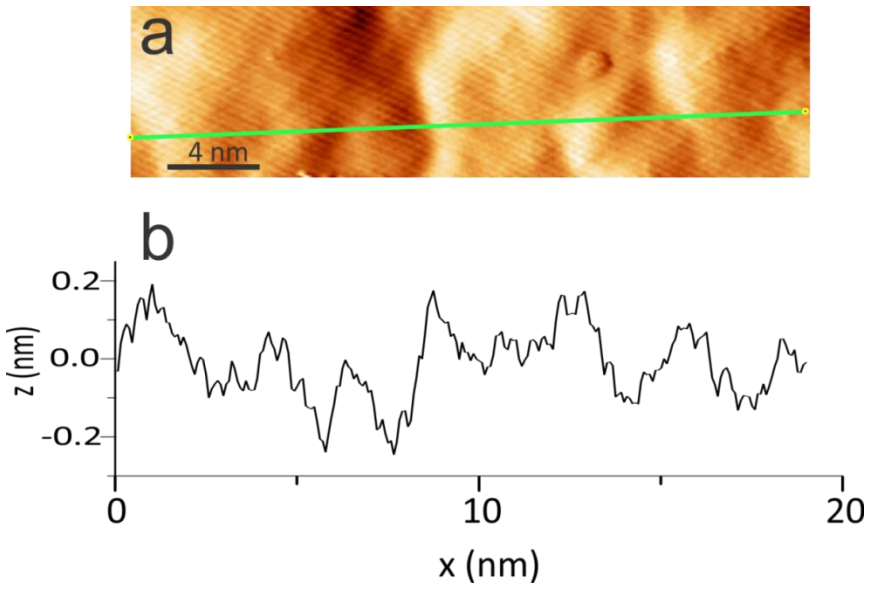

Figure S7: (a) STM image of a H_2Pc monolayer on top of the graphene device. (b) STM line scan along the green line in (a).

SI 8: Calculated influence of molecular orientation on activation energies

In figure 4b we present the activation barriers for different tilting angles α of a molecular configuration, in which both trans states are geometrically equivalent and therefore energetically degenerate (figure S8.1a), even if an electric field E is applied. We call this configuration "symmetric" in the following and always assume that all electric fields are oriented parallel to the z-axis. If we rotate the molecule now by 45° around the z-axis through its center prior to tilting around the x-axis, we arrive at an "asymmetric" configuration, in which the trans states are no longer equivalent for $\alpha \neq 0$ and $E \neq 0$ (figure S8.1b). We therefore refer to these states as trans1 and trans2. They correspond to the 1st and the 15th NEB image, respectively (see figure 4b). For trans1 both H atoms lie on the tilting axis, whereas for trans2 they are located perpendicular to the tilting axis. In the latter case the difference in the z-coordinates of the two H atoms is maximized. Therefore, any electrical polarization induced by the applied electric field inside the molecule should have its maximal impact on the state trans2. All other orientations can be seen as intermediate to the symmetric and asymmetric case.

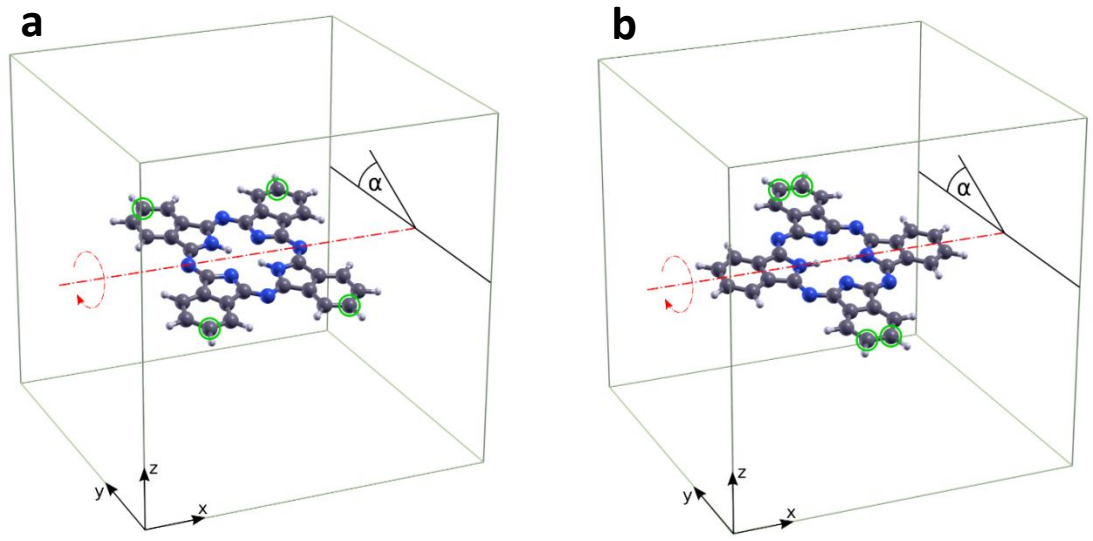

Figure S8.1: Simulated unit cell for the (a) symmetric and (b) asymmetric configurations. The tilting axis is represented by a dotted red line. In the experiment the rotation of the molecule in the applied electric field is naturally suppressed by the stabilizing interaction between the molecule and the supporting graphene substrate. Since the graphene sheet is missing in our calculations, artificial boundary conditions are used to mimic the anchoring of the molecule to the surface. Thus the *z*-coordinates of those four C atoms marked with green circles were constrained to prevent any rotation in the applied field during geometry optimizations, while the positions of the remaining atoms were optimized.

To see how molecular orientation with respect to the applied electric field affects activation barriers, we performed a set of NEB calculations also for the asymmetric situation. In analogy to trans1 and trans2, we name the two intermediate states inter1 and inter2. They correspond to the 5th and the 11th NEB image, respectively. We define the activation energy for the tautomerization as E_a=max(E_{inter1},E_{inter2})-min(E_{trans1},E_{trans2}) to quantify the maximal barrier in a forward and reverse transition between trans1 and trans2. Our data shows that E_{inter1}>E_{inter2} and E_{trans1}>E_{trans2} for all electric field strengths, which means that the activation barrier is E_a=E_{inter1}-E_{trans2}. In figure S8.2a we plot E_a as a function of the applied electric field and for different tilt angles. The trends are identical to figure 4b, since the activation barrier basically decreases with increasing field strength. The comparison also shows that the activation barrier of the asymmetric configuration is less sensitive to E. In figure S8.2b we show how the difference E_{trans1}-E_{trans2} depends on the applied field for different molecular tilt angles. As expected, we observe that this difference increases with E and α.

Let us discuss a technical aspect. We find an unexpected difference in the total energy between trans1 and trans2 (figure S8.2b) for α>0, even when no field is applied. For instance for α=20° we obtain E_{trans1}-E_{trans2}≈2.8 meV, which is small, but the difference should actually vanish. We attribute this artifact to the geometrical constraints imposed on the outer carbon atoms, as discussed in connection with figure S8.1.

While a fixed *z*-coordinate means that atoms can move freely in the molecular plane for α=0, this is not so for $\alpha \neq 0$. Therefore the geometrical constrains act slightly differently in the particular NEB calculations, depending on the molecular tilt. This effect may also cause E_{inter1}-E_{trans2} in figure S8.2a or E_a in figure 4b to deviate from a common value at E=0 for different α. In addition to this effect, for α=0 we see an approximately linear increase of E_{trans1}-E_{trans2} up to 1 meV as the applied electric field increases, shown in figure S8.2b. After careful checks of the geometries we believe that it is caused by numerical errors. Thus, we estimate that the overall numerical uncertainty of our NEB calculations is below 4 meV for the asymmetric configuration. However, it is important to note that this numerical uncertainty does not have an impact on our central statements. In particular, we find that the unexpected offsets in the symmetric configuration are much smaller than in the asymmetric one. Thus, at E=0 for different α, numerical errors are below 0.2 meV in the symmetric configuration, and for α=0 and different E they are below 1 meV (data not shown).

Another contribution to the deviations in E_{trans1}-E_{trans2} at E=0 with respect to different tilting angles could arise from dipole interactions of the periodic images of the molecule, which is an inherent shortcoming of the periodic DFT implementation. We recalculated the system's inter1 and trans2 states at α =20° and E=0 for a unit cell with doubled lattice constant (i.e., an eightfold unit cell volume). The energy difference $E_{inter1} - E_{trans2}$ dropped from 489.45 to 488.16 meV by 1.29 meV. However, the energy difference due to the dipole interaction is too small to explain the observed reduction in figure S8.2a.

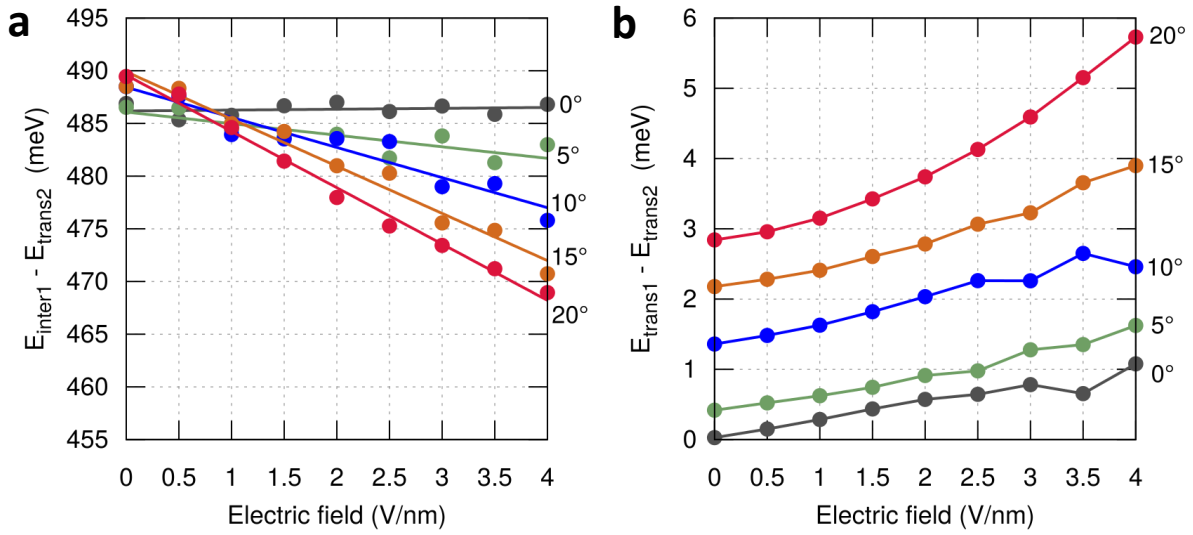

Figure S8.2: (a) Activation barrier for the tautomerization reaction and (b) total energy difference of trans1 and trans2 states for the asymmetric configuration, respectively.

SI 9: Calculated shift of the Dirac point as a function of the surface charge

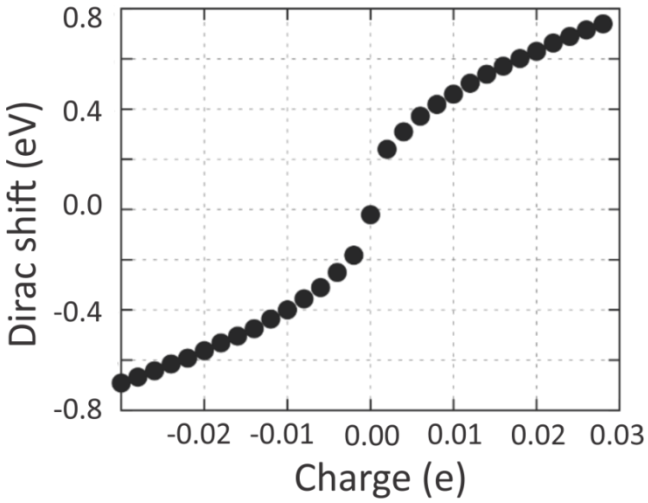

Figure S9: DFT calculation showing the shift of the Dirac point as a function of the charge on bare graphene, i.e. without any molecules. The charge is counted per primitive cell, containing two carbon atoms, and is compensated by a back-gate located around 5.9 Å below the graphene. [4]

SI 10: Calculated effect of charge accumulation on the activation barrier

An applied gate voltage leads to charge accumulation on the graphene layer and thereby also partially on the deposited molecules. To estimate the influence of the accumulated charge on the tautomerization reaction, we calculated the activation energies for a range of unit cell charges between -0.2*e* and 0.2*e* (where $e=|e|$ is the elementary charge). As visible in figure S10.1, this unit cell contains both the H_2Pc molecule and the graphene substrate. Indeed, there are $N_{pc}=64$ primitive cells of graphene in the unit cell.

Let us estimate the maximum amount of charge per primitive two-atom cell of graphene as realized in our experiments. From figure S2 we conclude that the Dirac point shifts by around 0.3 eV for the maximally applied back-gate voltage of 40 V. Considering figure S9, this corresponds to about 0.003*e* per primitive cell of graphene. Multiplied with $N_{pc}=64$, we expect a maximum deviation of the unit cell shown in figure S10.1 from neutrality by ±0.192*e*.

We explored a range of charges per unit cell between ±0.2*e* that is similar to the experimentally derived value, as displayed in figure S10.2. Electric fields were assumed to be constant and to take values up to the maximum strength estimated in section SI 5. From our calculations we expect that charge accumulation has an effect of less than 4 meV on activation barriers.

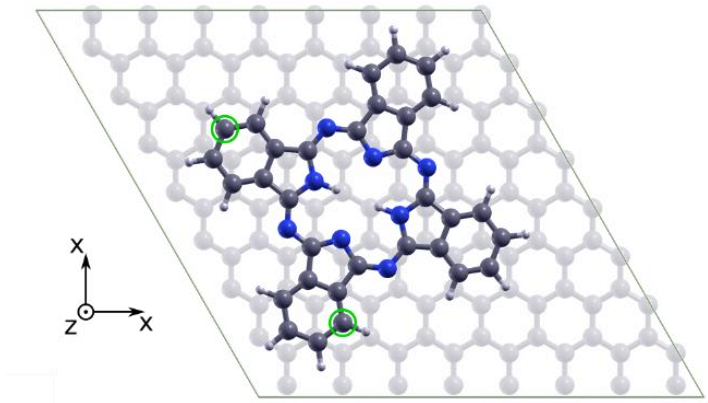

Figure S10.1: Simulated unit cell containing the H_2Pc molecule on top of a graphene sheet. We restricted the *x*- and *y*-coordinates of two outer carbon atoms of the molecule, marked by the green circles, to prevent it from wandering around on the graphene surface during structural relaxations under different charge and electric field conditions. The back-gate was introduced into the DFT calculations as a charged plane at a distance of 5.4 Å below the graphene sheet. [4]

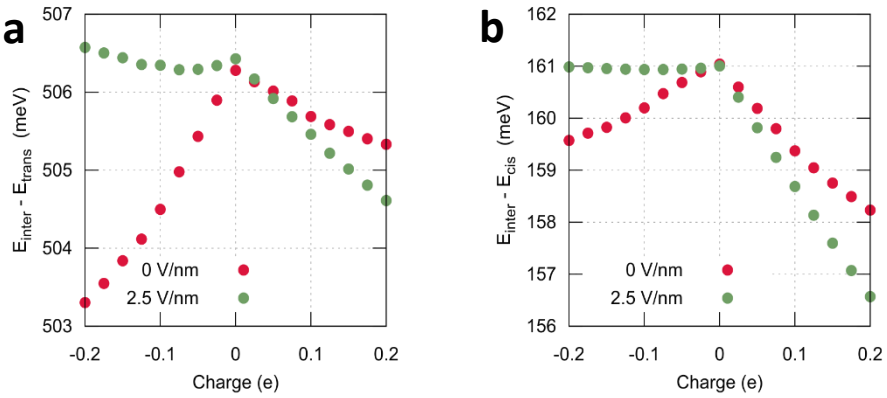

Figure S10.2: Variation of activation barriers with the total charge of the simulated unit cell at electric field strengths of 0 and 2.5 V/nm.

SI 11: Calculated shift of molecular orbital energies with gate voltage

It is well-known that the molecular energy levels at the surface of a graphene device can be tuned by applying a back-gate voltage.[5-6] When the energy of the molecular orbitals is shifted in this manner, the number of electrons which can activate the intramolecular hydrogen transfer through charge injection from the tip into unoccupied electronic states of H_2Pc will be changed. Consequently, the bias voltage dependence of the reaction rate will be modified. Our theoretical calculations in figure S11 show that the molecular frontier orbitals shift monotonically, as the applied gate voltage is increased. Since the experimentally determined reaction rate is reduced symmetrically, it is insensitive to the polarity of the

applied back-gate voltage. Thus, the energy level shift cannot be the important factor for the reduction of the reaction rate.

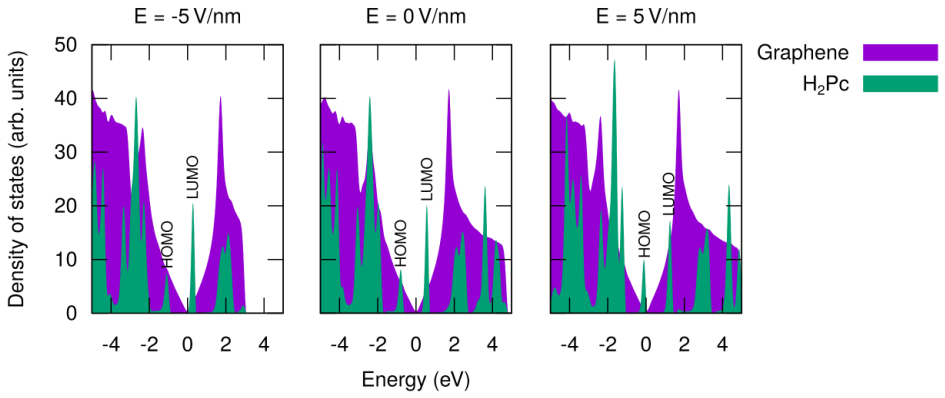

Figure S11: Local density of states of H_2Pc on graphene. The HOMO and LUMO of the molecule are shifted relative to the density of states of graphene as a result of an applied electric field.

References

1. Zhang, Y.; Brar, V. W.; Wang, F.; Girit, C.; Yayon, Y.; Panlasigui, M.; Zettl, A.; Crommie, M. F., Giant phonon-induced conductance in scanning tunnelling spectroscopy of gate-tunable graphene. *Nat. Phys.* **2008,** *4* (8), 627-630.
2. Castro Neto, A. H.; Guinea, F.; Peres, N. M. R.; Novoselov, K. S.; Geim, A. K., The electronic properties of graphene. *Rev. Mod. Phys* **2009,** *81* (1), 109-162.
3. Cortina, H.; Senent, M. L.; Smeyers, Y. G., Ab Initio Comparative Study of the Structure and Properties of H2-Porphin and H2-Phthalocyanine. The Electronic Absorption Spectra. *J. Phys. Chem. A* **2003,** *107* (42), 8968-8974.
4. Brumme, T.; Calandra, M.; Mauri, F., Electrochemical doping of few-layer ZrNCl from first principles: Electronic and structural properties in field-effect configuration. *Phys. Rev. B* **2014,** *89* (24), 245406.
5. Bouvron, S.; Maurand, R.; Graf, A.; Erler, P.; Gragnaniello, L.; Skripnik, M.; Wiedmann, D.; Engesser, C.; Nef, C.; Fu, W., et al., Charge transport in a single molecule transistor probed by scanning tunneling microscopy. *Nanoscale* **2018,** *10* (3), 1487-1493.
6. Riss, A.; Wickenburg, S.; Tan, L. Z.; Tsai, H.-Z.; Kim, Y.; Lu, J.; Bradley, A. J.; Ugeda, M. M.; Meaker, K. L.; Watanabe, K., et al., Imaging and Tuning Molecular Levels at the Surface of a Gated Graphene Device. *ACS Nano* **2014,** *8* (6), 5395-5401.